The Astrophysical Journal, 961:61 (6pp), 2024 January 20 https://doi.org/10.3847/1538-4357/ad0da9

HESS J1809-193: Gamma-Ray Emission by Cosmic Rays from a Past Explosion

Sovan Boxi[1] and Nayantara Gupta[1]
Raman Research Institute, C.V. Raman Avenue, 5th Cross Road, Sadashivanagar, Bengaluru, Karnataka 560080, India; sovanboxi@rrimail.rri.res.in, nayan@rri.res.in
Received 2023 September 7; revised 2023 October 30; accepted 2023 November 12; published 2024 January 15

Abstract

The very-high-energy γ-ray source HESS J1809-193 has been detected by the LHAASO and HAWC observatory beyond 100 TeV energy. It is an interesting candidate for exploring the underlying mechanisms of γ-ray production due to the presence of supernova remnants, pulsars, and molecular clouds close to it. We have considered the injection of the energetic cosmic rays from a past explosion, whose reminiscent may be SNR G011.0-00.0, which is located within the extended γ-ray source HESS J1809-193. We explain the multiwavelength data from the region of HESS J1809-193 with synchrotron, inverse Compton, and bremsstrahlung emission of cosmic-ray electrons and secondary γ-ray production in interactions of cosmic-ray protons with the cold protons in the local molecular clouds within a time-dependent framework including the diffusion loss of cosmic rays. The observational data have been modeled with the secondary photons produced by the time-evolved cosmic-ray spectrum assuming the age of the explosion is 4500 yr.

Unified Astronomy Thesaurus concepts: High energy astrophysics (739); Gamma-rays (637); Supernova remnants (1667)

1. Introduction

Ground-based γ-ray detectors like High Energy Stereoscopic System (H.E.S.S.), Major Atmospheric Gamma Imaging Cherenkov, Tibet, High Altitude Water Cherenkov (HAWC), Large High Altitude Air Shower Observatory (LHAASO), and space-based γ-ray detectors like Fermi Large Area Telescope (LAT) and AGILE are exploring the γ-ray sky in different energy windows and revealing the very energetic cosmic accelerators in our Galaxy and beyond. They complement each other in providing us the γ-ray data covering energies from a few tens of MeV to thousands of PeV, and along with the observations at lower frequencies (radio, infrared, optical, ultraviolet, and X-ray), it is possible to build up the spectral energy distributions (SEDs) to probe the nature of these sources. H.E.S.S. is an array of high-energy imaging atmospheric Cherenkov telescopes operating in Khomas Highland in Namibia. The Galactic plane survey by the HESS Collaboration has revealed a large population of γ-ray sources in the very-high-energy regime (HESS Collaboration et al. 2018). Many of them are either pulsar wind nebulae (PWNs) or supernova remnants (SNRs) or composite systems. The extended γ-ray sources are particularly interesting in this field because it is challenging to identify the different types of sources and different types of radiative mechanisms responsible for the emission in different energy regimes.

The discovery of HESS J1809-193 was reported for the first time in Aharonian et al. (2007). They discussed that the source HESS J1809-193 is located about $0^{\circ}.2$ east of the pulsar PSR 1809-1917, which can power it with an efficiency of only 1.2%, assuming the γ-ray source is entirely powered by this pulsar. The possibility that it is powered by SNR G011.0-00.0 (Bamba et al. 2003) in the X-ray frequency range was also mentioned in this paper. Subsequently, the origin of its emission has been debated in various works due to the presence of SNRs, molecular clouds (MCs), and a pulsar close to the emission region. This source has been observed above 56 TeV and possibly above 100 TeV by HAWC (Abeysekara et al. 2020; Goodman 2022). Very recently, LHAASO detected this source with a significance greater than 4σ at an energy exceeding 100 TeV. In the first LHAASO catalog, this source has been reported as an ultra-high-energy source, designated as 1LHAASO J1908+0615u (Cao et al. 2023). It was also suggested earlier that the pulsar PSR J1809-1917 powers the X-ray PWN of extension $3'$ (Kargaltsev & Pavlov 2007; Anada et al. 2010; Klingler et al. 2018, 2020).

Castelletti et al. (2016) discovered a system of MCs at the edge of the shock front of the SNR G011.0-00.0 associated with HESS J1809-193. They suggested that the most likely origin of the very-high-energy γ-ray emission is collison of ions accerelated by the SNR in the MCs.

Araya (2018) modeled the extended GeV emission of HESS J1809-193 with steady-state hadronic and leptonic emissions without including the diffusion loss of the cosmic rays. The author included the contributions from the three SNRs: SNR G011.0-00.0, SNR G11.1+0.1, and SNR G11.4-0.1 to explain the GeV γ-ray data considering the interactions of cosmic-ray protons with the local MCs in the hadronic model and the bremsstrahlung emission in the leptonic model; however, the very-high-energy γ-ray data were explained in both cases with the inverse Compton (IC) emission of the relativistic electrons.

Recently, HESS Collaboration et al. (2023) did a detailed observational and theoretical analysis and identified the two components, component A and B, of this source. Component A is more extended in space and has a higher γ-ray flux than component B. They did a time-dependent leptonic modeling of HESS J1809-193 including the effect of diffusion loss of the electron and positron pairs injected by the pulsar PSR 1809-1917. The pulsar halo model was used considering two populations of leptons having different ages to explain the multiwavelength SED. The possibility of hadronic origin

[1] Corresponding author.

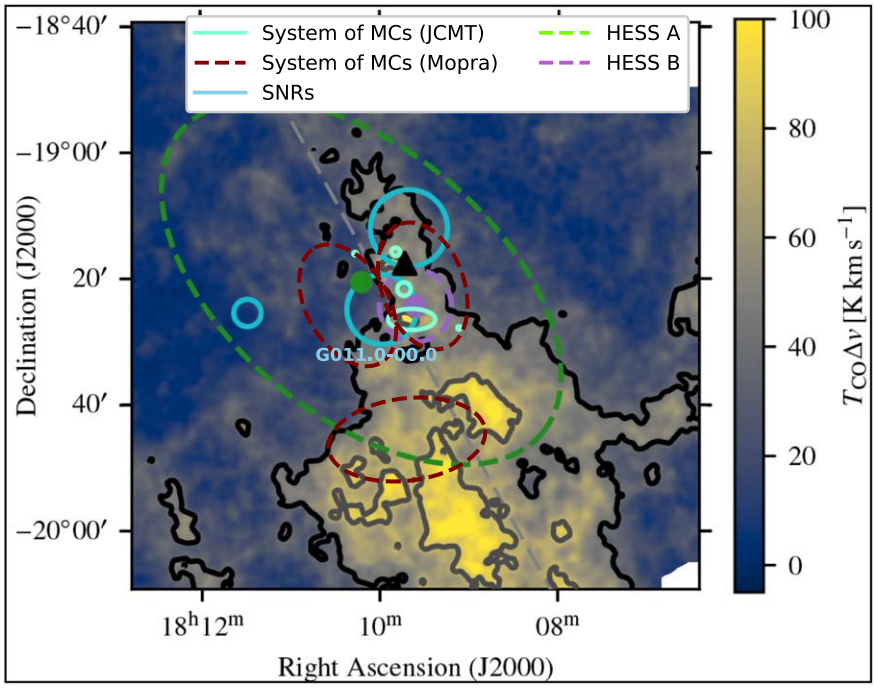

Figure 1. Positions of SNRs (sky blue circles), FUGIN Map (Umemoto et al. 2017), pulsar PSR J1809-1917 (black triangle), HESS A (green dot and dashed contour), HESS B (purple dot and dashed contour), and their 1σ contours from Figure D1 of HESS Collaboration et al. (2023). We have superposed the positions of MCs from the JCMT (Castelletti et al. 2016) and Mopra (Voisin et al. 2019) observations on the same plot. The Mopra observation shows three extended MCs with maroon dashed contours. The JCMT observation of MCs due to a CO ($J = 3$–2) tracer is shown as an aquamarine contour.

of γ-rays is also discussed in this paper within a steady-state scenario.

Li et al. (2023) used Chandra X-ray data to model the SED with a leptonic model. They found that a magnetic field of 21 μG is needed to explain the extended X-ray halo observed from HESS J1809-193. Due to the high synchrotron emission, IC emission of the pairs is suppressed; hence, it is hard to explain the very-high-energy γ-ray data with the leptonic model.

We have done a time-dependent modeling including the diffusion loss of cosmic rays injected at the site of the source from a past explosion. The secondary photons generated in radiative losses of the cosmic-ray electrons and hadronic interactions of cosmic-ray protons are used to model the multiwavelength spectrum of HESS J1809-193. It is shown here that the very-high-energy γ-ray components A and B identified in HESS data can be explained in our model by hadronic and leptonic interactions, respectively.

2. HESS J1809-193

HESS J1809-193 is an extended TeV γ-ray source located at R.A. (J2000) $= 18^{h}10^{m}31^{s} \pm 12^{s}$, decl. (J2000) $= -19°18' \pm 2'$ (Aharonian et al. 2007). As discussed above, HESS Collaboration et al. (2023) have modeled this source with two components: the extended asymmetric component as HESS A with 1σ radius of extension of the major and minor axis $0.^{\circ}613$, $0.^{\circ}351$, respectively and the symmetric compact component as HESS B with 1σ radius of extension $0.^{\circ}0953$ (see Figure 1). Pinpointing the exact counterpart for this source poses a considerable challenge, owing to the presence of several potential associations juxtaposed within the depicted region in Figure 1. For instance, radio observation at 330 and 1456 MHz reveals that the region harbors at least two SNRs within the extension of the source, notably G011.1 +00.1 and G011.0-00.0 (Green 2004; Brogan et al. 2006; Castelletti et al. 2016). The specific distance of G011.1+00.1 remains unknown as of now. The estimated distance of G011.0-00.0 (Bamba et al. 2003) is 2.6 kpc; 2.4 ± 0.7 kpc (Shan et al. 2018). Unfortunately, the age for SNR G011.0-00.0 is still unresolved (Araya 2018). The presence of the energetic pulsars PSR J1811-1925 ($\dot{E} = 6.4 \times 10^{36}$ erg s^{-1}, $d \sim 5$ kpc) and PSR J1809-1917 ($\dot{E} = 1.8 \times 10^{36}$ erg s^{-1}, $d \sim 3.3$ kpc; Manchester et al. 2005) adds more complexity to the picture. A handful of MCs within the line of sight of the emission region has been independently identified by Castelletti et al. (2016) and Voisin et al. (2019). We have shown the SNRs and the MCs in Figure 1 along with the pulsar PSR J1809-1917. ^{12}CO(3–2) observations carried out by Castelletti et al. (2016) using the James Clerk Maxwell Telescope (JCMT; Maunakea, Hawaii) reveal a substantial overlap between the primary emission region of the HESS source and MC system. Deep radio observation around the source using the Karl G. Jansky Very Large Array by the same group also confirms a strong spatial correlation between the shock front of the SNR G011.0-00.0 and MC system. Using H I 21 cm absorption technique and ^{12}CO emission they estimated the distance of the MCs and by H I absorption the distance of SNR G011.0-00.0 and subsequently established a physical connection between them. The average distance of this cloud system as well as the associated SNR as quoted there is $\approx$3 kpc. The predicted mass of each individual cloud varies from 7×10^{2}–1.3×10^{3} $M_{\odot}$ for velocity 21 km s^{-1} (Castelletti et al. 2016, Table 2). Likewise, the intensity map CS(1–0) using Mopra Telescope (Voisin et al. 2019) covering various local standard-of-rest velocities of molecular material unveils the existence of clumps of MCs stretched over the vicinity of SNRs and the emission region. Depending on the tracer selected, the mass of the individual cloud differs, ranging from 10^{3} to 2.3×10^{5} $M_{\odot}$. In similar

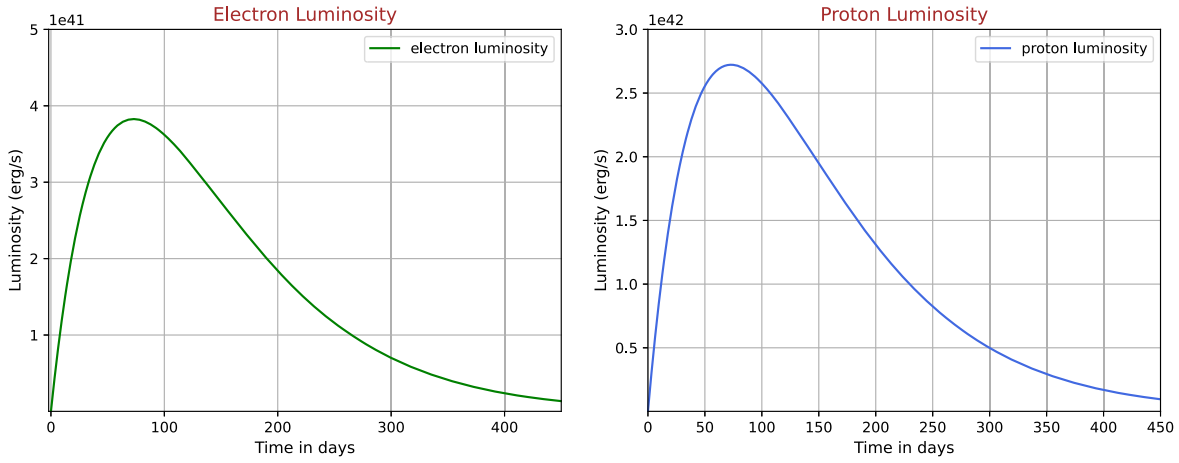

(a) (b)

Figure 2. Time evolution of injected luminosity in electrons (a) and protons (b).

fashion, molecular hydrogen density varies from 150 cm^{-3} to 4.4×10^4 cm^{-3} (Table D.1 of Voisin et al. 2019). We have presented an intensity map superposing the JCMT (Castelletti et al. 2016) and Mopra (Voisin et al. 2019) observations over FUGIN map (Umemoto et al. 2017) in Figure 1.

It is evident from our Figure 1 as well as the discussion above that the molecular hydrogen density varies by orders of magnitude over the entire emission region. The spatial variation in matter distribution in the region of HESS J1809-193 suggests the interaction of SNR shock, and MCs may have an important role in powering this source. The cosmic-ray protons lose energy slower than the cosmic-ray electrons, so they can propagate to longer distances before losing energy and may produce extended emission (HESS component A) in very-high-energy γ-rays, while cosmic-ray electrons can emit very-high-energy γ-rays by the IC mechanism and produce HESS component B of HESS J1809-193 (HESS Collaboration et al. 2023).

3. SED Modeling

In this section, we discuss the modeling of the observed multiwavelength spectrum in the region of HESS J1809-193. The cosmic rays are accelerated in supernova shocks by diffusive shock acceleration (Blandford & Eichler 1987) mechanism. We have assumed that the supernova explosion at the location of the source lasted for nearly a year and injected very-high-energy cosmic-ray electrons and protons, which have power-law distributions in energy. Subsequently, they lose energy in the ambient magnetic field, radiation field, and matter, and some escape from the emission region. The transport equation is given below, used to calculate the time-evolved cosmic-ray electron and proton spectra. The electrons are losing energy by synchrotron emission in the local ambient magnetic field and IC emission in the local interstellar radiation field (ISRF) and cosmic-microwave background (CMB) radiation. The electrons also lose energy by bremsstrahlung emission in the MCs. The protons are losing energy mainly in proton–proton interactions with the MCs. The densities of the MCs vary by several orders of magnitude over the emission region; hence, we have used an average value to fit the observed γ-ray data. We have used the GAMERA code (Hahn et al. 2022) to calculate the time-evolved cosmic-ray particle spectra, including all the energy loss processes and the escape of cosmic rays, and subsequently the nonthermal emission covering radio to very-high-energy γ-ray frequencies from the time-evolved particle spectra. The transport equation used to study the time evolution of the relativistic electrons or protons is given by

$$\frac{\partial N(E,t)}{\partial t} = Q(E,t) - \frac{\partial [b(E,t)N(E,t)]}{\partial E} - \frac{N(E,t)}{t_{\rm diff}}, \quad (1)$$

where $N(E, t)$ is the resulting particle spectra at any time t, $Q(E, t)$ is the injection spectra, and $b = b(E, t)$ represents the energy loss of particles. The exact forms of the time-dependent injected luminosity in electrons and protons are shown separately in Figures 2(a) and (b), respectively. In the GAMERA framework, the complete Klein–Nishina cross section for IC scattering (Blumenthal & Gould 1970) is utilized to compute the photon flux resulting from the relativistic electrons. For calculating the IC emission from the ISRF target photon field, we have used the distribution of ISRF as given in Popescu et al. (2017). The code calculates the bremsstrahlung radiation for both electron–electron and electron–ion interactions. For proton–proton interactions, GAMERA uses semi-analytical parameterization developed by Kafexhiu et al. (2014). In our calculation, we have incorporated the GEANT 4.10.0 hadronic interaction model for proton–proton interaction. We have included the energy-dependent diffusion loss of cosmic-ray electrons and protons using the following form of diffusion coefficient:

$$D = D_0 \left(\frac{E}{E_0} \right)^{\delta}, \quad (2)$$

where $D_o = 1.1 \times 10^{28}$ cm^2 s^{-1} is the diffusion coefficient normalized at $E_0 = 40$ TeV and $\delta = 0.58$ following HESS Collaboration et al. (2023). They fitted the observed size of component A with the help of the GAMERA library (Hahn et al. 2022) and the best-fit model provides the value for δ, D_o (HESS Collaboration et al. 2023); this value of D_o is similar to that reported in earlier work (Abeysekara et al. 2017). We have used these best-fit values in our calculation. The diffusion-loss mechanism of particles (electrons and protons) has been included through the diffusion timescale $t_{\rm diff}$ in the transport

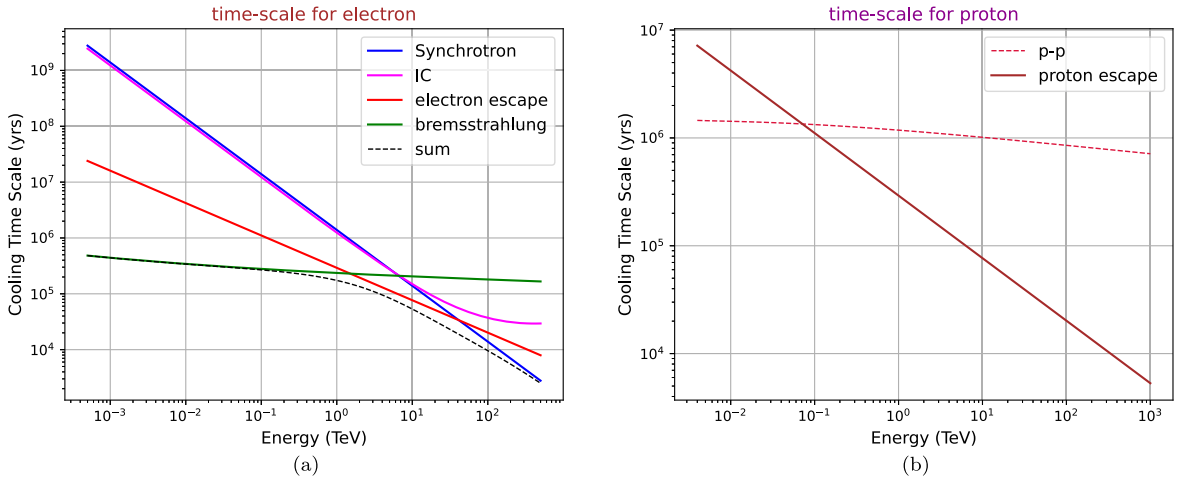

Figure 3. Energy loss timescales of electrons (a) and protons (b).

equation. The diffusion timescale $t_{\rm diff}$ can be expressed in terms of the diffusion coefficient D and the size of the region where the cosmic rays are trapped and lose energy, which we assume to be the same as the size of the emission region:

$$t_{\rm diff} = \frac{L_{\rm emission}^2}{D}. \quad (3)$$

In the above equation, we assume $L_{\rm emission}$ to be the total extension of the emission region observed by HESS, which is approximately 37 pc. The escape and cooling timescales of electrons and protons have been shown in Figures 3(a) and (b), respectively, for the regions near HESS J1809-193. At higher energy, synchrotron cooling of electrons dominates over other energy loss processes. The diffusion loss of protons is very important above 100 GeV energy as the diffusion-loss timescale decreases rapidly with increasing energy. The age of the explosion is adjusted along with the other parameters listed in Table 1 to fit the SED shown in Figure 4.

4. Results

Figure 1 strongly suggests association between SNRs and the MC system. We have used this association in modeling the source HESS J1809-193 within a time-dependent framework. We have assumed that SNR G011.0-00.0, whose age is not known, exploded thousands of years ago and cosmic-ray electrons and protons were injected in the region of HESS J1809-193 from this explosion. The cosmic rays have cooled down by interactions with the ambient magnetic field, radiation field, and matter distributed near the SNR. The cosmic-ray electrons have lost their energy through synchrotron radiation, through IC with the CMB and ISRF photon field, and through bremmstrahlung emission, and the cosmic-ray protons have lost energy in proton–proton interactions with the ambient hydrogen molecules. The synchrotron self-Compton emission is very low compared to the emission from the other processes, but it has been included in our work.

We have also assumed that the injection luminosity was time varying and the injection of cosmic rays continued for a year. The precise form of the injected luminosity used in this work has been shown in Figure 2. We have used the publicly available software GAMERA to calculate the time-evolved cosmic-ray spectrum and photon spectrum at present day after including radiative losses of electrons, hadronic interactions, and diffusion loss of cosmic rays. The radiation spectra of electrons and protons vary with the explosion's age and the total energy injected during the explosions. After adding the leptonic and hadronic contributions, the values of these parameters are varied so that the total SEDs fit the observed spectra. In Figure 4, we show the total SEDs and the individual components in our lepto-hadronic model. The values of the parameters used in our model are listed in Table 1. The following spectral distributions of injected cosmic rays: (a) electrons: $\frac{dN_e}{dE_e} \propto E_e^{-2.4}$ and (b) protons: $\frac{dN_p}{dE_p} \propto E_p^{-2}$ have been adapted to fit the SEDs. The total amount of energy injected into particles throughout the age of the source to explain the observed data at the present day is (a) $W^p = 4.67 \times 10^{49}$ erg for the cosmic-ray protons and (b) $W^e = 6.56 \times 10^{48}$ erg for the cosmic-ray electrons; their sum is only a few percent of the kinetic energy released in a canonical supernova explosion $\sim 10^{51}$ erg (Ginzburg & Ptuskin 1975).

Table 1
Parameters Used for Modeling HESS J1809-193

Parameters	HESS J1809-193
Energy injected in protons	4.67×10^{49} erg
Energy injected in electrons	6.56×10^{48} erg
Maximum energy of protons injected	10^3 TeV
Minimum energy of protons injected	4×10^{-3} TeV
Maximum energy of electrons injected	5×10^2 TeV
Minimum energy of electrons injected	5×10^{-4} TeV
Spectral index of injected proton spectrum	-2
Spectral index of injected electron spectrum	-2.4
Number density of particles in MC	50 cm^{-3}
Magnetic field in emission region	3 μG
Distance of MC	2.6 kpc
Age of explosion	4500 yr

As shown in Figure 4 the radio data points from SNR G011.0-00.0 can be well explained by the synchrotron emission from the cosmic-ray electrons in our model. The synchrotron emission in the X-ray band passes through the butterfly region of the Suzaku observation but does not cover the entire region. Fermi-LAT data have been fitted using the bremmstrahlung emission of the cosmic-ray electrons in MCs and proton–proton interactions. The HESS data points for the B component can be explained with IC emission of the cosmic-

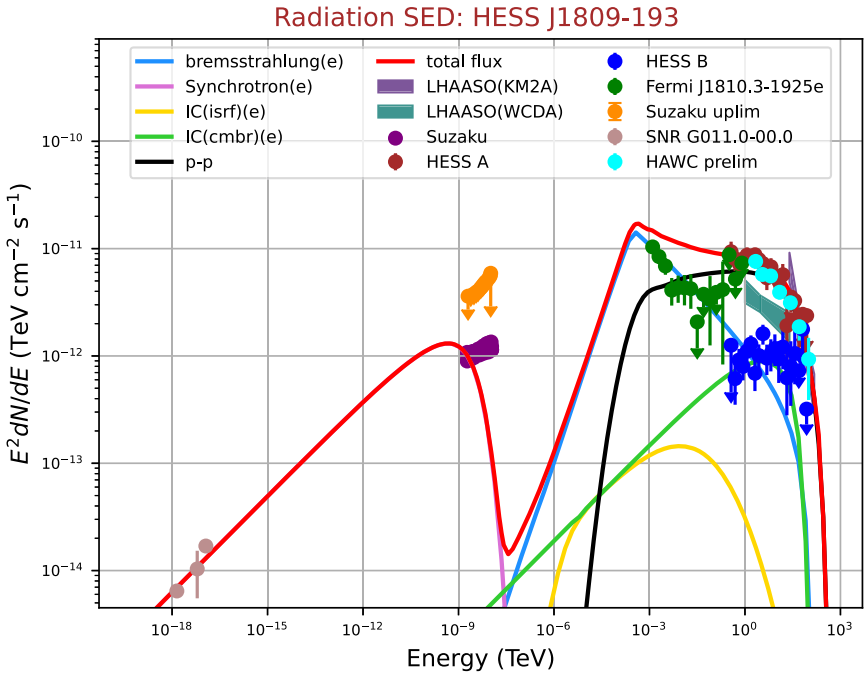

Figure 4. Multiwavelength SED of HESS J1809-193. Data points from different observations: Fermi-LAT in green dots (HESS Collaboration et al. 2023); two-component HESS data: HESS A in brown and HESS B in blue (HESS Collaboration et al. 2023); HAWC preliminary data in cyan (Goodman 2022); LHAASO: WCDA data between 1 and 25 TeV in teal butterfly and KM2A data beyond 25 TeV in purple butterfly (Cao et al. 2023); X-ray data from Suzaku: butterfly in violet and upper limit in orange (Anada et al. 2010); radio data for SNR G011.0-00.0 in light brown (Brogan et al. 2006).

ray electrons and the extended A component with proton–proton interactions. The HAWC data points, HESS data points for the A component, and LHAASO KM2A data points overlap with each other, and they are well fitted with hadronic interactions in our model. LHAASO WCDA data points near 25 TeV partially overlap with the HESS data points for the A component. At lower energy, the LHAASO WCDA data points are in between the data points of B and A components of HESS. Thus it is possible to fit most of the γ-ray data points with a single source; however, it is also possible that more than one source may contribute to the observed emission as there are multiple sources in the region of HESS J1809-193.

5. Discussion and Conclusion

HESS J1809-193 is an interesting source to study the multiwavelength emission mechanisms in the particle acceleration site due to the availability of sufficient observational data covering radio to hundred TeV γ-ray energy from different observatories. SNRs, pulsars, and MCs are present at the location of the source; this association suggests different possible scenarios for the underlying emission mechanisms. Earlier works have considered leptonic (Aharonian et al. 2007; HESS Collaboration et al. 2023) models to explain the multiwavelength data with the electrons emitted by the pulsar, and also the hadronic model has been applied to explain the source HESS J1809-193 within a steady-state scenario (Araya 2018).

We have suggested that the explosion of SNR G011.0-00.0 may be the origin of HESS J1809-193. We have explained the multiwavelength data within a time-dependent framework after including all the energy loss processes and the diffusion loss of cosmic rays. In our model the maximum energy of the injected protons is higher than the maximum energy of the injected electrons because the electrons cool down much faster than the protons, and it is much harder to accelerate the electrons to very high energy. Since protons lose energy slowly and propagate to a longer distance before losing energy, they are expected to give the emission from the extended region at the highest observed energy. It has been discussed earlier that the spatial distribution of the MCs is not reflected in the extended γ-ray emission observed by HESS (HESS Collaboration et al. 2023). We note that the energy-dependent diffusion timescale of the cosmic-ray protons is much shorter than the proton−proton interaction timescale at very high energy, and due to this reason the distribution of the protons is not uniform in the emission region; as a result, the γ-ray emission may not trace the distribution of MCs. It would be possible to study the morphology and the distribution of γ-ray emission at the site of HESS J1809-193 in more detail with more observational data in future. There may be multiple sources working together at the site of HESS J1809-193, and the role of the pulsar PSR J1809-1917 to produce a pulsar halo may be important. Our work presents an alternative scenario to explain HESS J1808-193.

Acknowledgments

The authors thank the referee for helpful comments.
Software: GAMERA (Hahn et al. 2022).

ORCID iDs

Sovan Boxi https://orcid.org/0009-0004-1305-9578
Nayantara Gupta https://orcid.org/0000-0002-1188-7503

References

Abeysekara, A., Albert, A., Alfaro, R., et al. 2017, Sci, 358, 911
Abeysekara, A. U., Albert, A., Alfaro, R., et al. 2020, PhRvL, 124, 021102

Aharonian, F., Akhperjanian, A. G., Bazer-Bachi, A. R., et al. 2007, A&A, 472, 489
Anada, T., Bamba, A., Ebisawa, K., & Dotani, T. 2010, PASJ, 62, 179
Araya, M. 2018, ApJ, 859, 69
Bamba, A., Ueno, M., Koyama, K., & Yamauchi, S. 2003, ApJ, 589, 253
Blandford, R., & Eichler, D. 1987, PhR, 154, 1
Blumenthal, G. R., & Gould, R. J. 1970, RvMP, 42, 237
Brogan, C. L., Gelfand, J. D., Gaensler, B. M., Kassim, N. E., & Lazio, T. J. W. 2006, ApJL, 639, L25
Cao, Z., Aharonian, F., An, Q., et al. 2023, arXiv:2305.17030
Castelletti, G., Giacani, E., & Petriella, A. 2016, A&A, 587, A71
Ginzburg, V. L., & Ptuskin, V. S. 1975, SvPhU, 18, 931
Goodman, J. 2022, 7th Heidelberg Int. Symp. on High-Energy Gamma-Ray Astronomy, ed. F. Aharonian, https://indico.icc.ub.edu/event/46/contributions/1375/
Green, D. A. 2004, BASI, 32, 335
Hahn, J., Romoli, C., & Breuhaus, M., 2022 GAMERA: Source Modeling in Gamma Astronomy, Astrophysics Source Code Library, ascl:2203.007
HESS Collaboration, Abdalla, H., Abramowski, A., et al. 2018, A&A, 612, A1
HESS Collaboration, Aharonian, F., Benkhali, F. A., et al. 2023, A&A, 672, A103
Kafexhiu, E., Aharonian, F., Taylor, A. M., & Vila, G. S. 2014, PhRvD, 90, 123014
Kargaltsev, O., & Pavlov, G. 2007, ApJ, 670, 655
Klingler, N., Kargaltsev, O., Pavlov, G. G., & Posselt, B. 2018, ApJ, 868, 119
Klingler, N., Yang, H., Hare, J., et al. 2020, ApJ, 901, 157
Li, C. M., Ge, C., & Liu, R. Y. 2023, ApJ, 949, 90
Manchester, R. N., Hobbs, G. B., Teoh, A., & Hobbs, M. 2005, AJ, 129, 1993
Popescu, C. C., Yang, R., Tuffs, R. J., et al. 2017, MNRAS, 470, 2539
Shan, S. S., Zhu, H., Tian, W. W., et al. 2018, ApJS, 238, 35
Umemoto, T., Minamidani, T., Kuno, N., et al. 2017, PASJ, 69, 78
Voisin, F. J., Rowell, G. P., Burton, M. G., et al. 2019, PASA, 36, e014